J|A|C|S ARTICLES

Published on Web 09/08/2009

pH-Induced Aggregation of Gold Nanoparticles for Photothermal Cancer Therapy

Jutaek Nam, Nayoun Won, Ho Jin, Hyokyun Chung, and Sungjee Kim*

Department of Chemistry, Pohang University of Science & Technology, San 31, Hyojadong, Namgu, Pohang 790-784, South Korea

Received March 17, 2009; E-mail: sungjee@postech.ac.kr

Abstract: We report a "smart" gold nanoparticle that is designed to aggregate in mild acidic intracellular environments by its hydrolysis-susceptible citraconic amide surface. With a relatively small size of 10 nm, the "smart" gold nanoparticles can be efficiently internalized into cancerous cells. Triggered by pH change, the nanoparticle surfaces are engineered to have both positive and negative charges. Electrostatic attractions between the nanoparticles can rapidly form aggregates inside the cells, and the aggregates accumulate as the exocytosis is blocked by the increased size. Endocytosis of gold nanoparticles and the aggregation are monitored real-time by dark field optical microscopy. The pH-induced formation of aggregates shifts the absorption to far-red and near-infrared. The absorption shift to longer wavelength is used for photothermal cancer therapy as it guarantees maximal tissue penetration for potential therapeutic applications. The gold nanoparticles show selective and efficient destruction of cancerous cells with an intensity threshold of 5 W/cm^2 to induce the thermal destruction. In the intensity range 5−13 W/cm^2, the circular area of damaged cells increases linearly with the irradiation power density. This shows a new proof-of-concept for photothermal cancer therapy that exploits collective plasmon modes of metal nanoparticles.

Introduction

Noble metal nanoparticles have attracted great interest due to their novel optical properties from surface plasmon resonances. Particularly, gold nanoparticles are being extensively studied for biological and medical applications such as colorimetric biosensors,[1,2] drug delivery,[3−5] cancer imaging,[6−10] and cancer therapies.[11−13] They allow simple and flexible synthetic routes and are considered relatively biocompatible. Gold nanoparticles can resonantly absorb and scatter incident light upon excitation of their surface plasmon oscillations typically in the visible range, with their absorption cross sections orders of magnitude larger than those of strongly absorbing organic molecules.[14] In addition, photon energies that are absorbed by gold nanoparticles can be efficiently converted into heat on a picosecond time scale, as a result of electron−phonon and phonon−phonon processes.[15] Gold nanoparticles can be a highly potent photothermal therapeutic agent, by exploiting their strong absorptions and efficient heat conversions. However, cancer phototherapies often suffer from limited tissue penetration, which confines their applicability mostly to melanoma. Photosensitizers that can absorb at longer wavelengths of far-red or near-infrared (NIR) have been constantly pursued to extend the penetration depth. For example, phthalocyanine derivatives that can absorb at extended wavelengths have been investigated for photodynamic therapies.[16] Since most gold nanoparticles have their optical resonances in the visible range, the resonances need to be engineered to longer wavelengths before they can be successfully used for anticancer photosensitizers. Surface plasmon resonances of metal nanoparticles are heavily governed by the size and shape of the nanoparticles. Various nanostructures that can absorb NIR are made, including gold nanorods,[17,18]

(1) Xu, X.; Han, M. S.; Mirkin, C. A. *Angew. Chem., Int. Ed.* **2007**, *46*, 3468–3470.
(2) Lee, J.-S.; Ulmann, P. A.; Han, M. S.; Mirkin, C. A. *Nano Lett.* **2008**, *8*, 529–533.
(3) Podsiadlo, P.; Sinani, V. A.; Bahng, J. H.; Kam, N. W. S.; Lee, J.; Kotov, N. A. *Langmuir* **2008**, *24*, 568–574.
(4) Chen, Y.-H.; Tsai, C.-Y.; Huang, P.-Y.; Chang, M.-Y.; Cheng, P.-C.; Chou, C.-H.; Chen, D.-H.; Wang, C.-R.; Shiau, A.-L.; Wu, C.-L. *Mol. Pharmaceutics* **2007**, *4*, 731–722.
(5) Paciotti, G. F.; Myer, L.; Weinreich, D.; Goia, D.; Pavel, N.; McLaughlin, R. E.; Tamarkin, L. *Drug Delivery* **2004**, *11*, 169–183.
(6) Sokolov, K.; Follen, M.; Aaron, J.; Pavlova, I.; Malpica, A.; Lotan, R.; Richards-Kortum, R. *Cancer Res.* **2003**, *63*, 1999–2004.
(7) Javier, D. J.; Nitin, N.; Levy, M.; Ellington, A.; Richards-Kortum, R. *Bioconjugate Chem.* **2008**, *19*, 1309–1312.
(8) Aaron, J.; Nitin, N.; Travis, K.; Kumar, S.; Collier, T.; Park, S. Y.; Jose-Yacaman, M.; Coghlan, L.; Follen, M.; Richards-Kortum, R.; Sokolov, K. *J. Biomed. Opt.* **2007**, *12*, 034007.
(9) Lee, S.; Cha, E.-J.; Park, K.; Lee, S.-Y.; Hong, J.-K.; Sun, I.-C.; Kim, S. Y.; Choi, K.; Kwon, I. C.; Kim, K.; Ahn, C.-H. *Angew. Chem., Int. Ed.* **2008**, *47*, 2804–2807.
(10) El-Sayed, I. H.; Huang, X.; El-Sayed, M. A. *Nano Lett.* **2005**, *5*, 829–834.
(11) Huang, X.; Jain, P. K.; El-Sayed, I. H.; El-Sayed, M. A. *Lasers Med. Sci.* **2008**, *23*, 217–228.
(12) Von Maltzahn, G.; Park, J.-H.; Agrawal, A.; Bandaru, N. K.; Das, S. K.; Sailor, M. J.; Bhatia, S. N. *Cancer Res.* **2009**, *69*, 3892–3900.
(13) Cheng, Y.; Samia, A. C.; Meyers, J. D.; Panagopoulos, I.; Fei, B.; Burda, C. *J. Am. Chem. Soc.* **2008**, *130*, 10643–10647.
(14) Link, S.; El-Sayed, M. A. *J. Phys. Chem. B* **1999**, *103*, 8410–8426.
(15) Link, S.; El-Sayed, M. A. *Int. Rev. Phys. Chem.* **2000**, *19*, 409–453.
(16) Miller, J. D.; Baron, E. D.; Scull, H.; Hsia, A.; Berlin, J. C.; McCormick, T.; Colussi, V.; Kenney, M. E.; Cooper, K. D.; Oleinick, N. L. *Toxicol. Appl. Pharmacol.* **2007**, *224*, 290–299.
(17) Kim, F.; Song, J. H.; Yang, P. *J. Am. Chem. Soc.* **2002**, *124*, 14316–14317.
(18) Jana, N. R.; Gearheart, L.; Murphy, C. J. *J. Phys. Chem. B* **2001**, *105*, 4065–4067.

Scheme 1. Synthesis of 4-(2-(6,8-Dimercaptooctanamido)ethylamino)-2-methyl-4-oxobut-2-enoic acid[a]

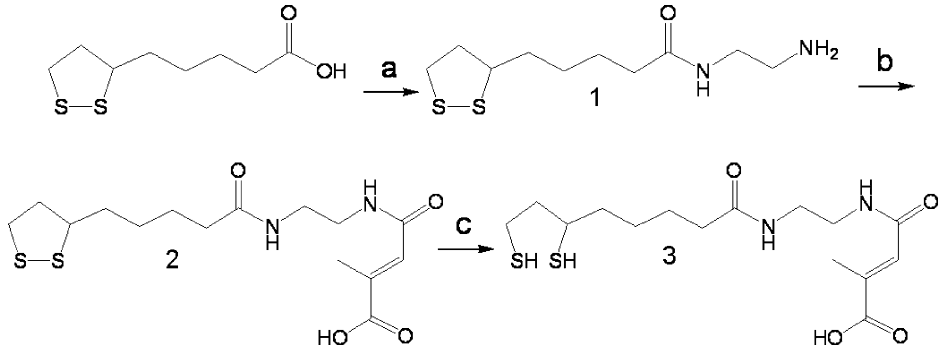

[a] (a) Ethylenediamine, 1,1-carbonyldiimidazole/anhydrous chloroform; (b) Citraconic anhydride/anhydrous chloroform; (c) Sodium borohydride/D.I. water.

gold nanoshells,[19] and gold nanocages.[20] They have also demonstrated photothermal therapeutic efficacy at NIR illumination.[21−24] However, they are relatively difficult to synthesize and may suffer from chemical contaminations from surfactants such as CTAB (Cetyltrimethylammonium bromide).[25] They are also relatively large in size reaching over 50 nm. The size may limit efficient endocytosis into cancerous cells and pose potential clearance problems when clinically tried. Recent studies have shown that gold nanoparticles of sizes larger than 50 nm begin to show rapidly reducing endocytosis efficiency.[26] Nanoparticles of hydrodynamic sizes larger than 20 nm are expected to have a circulation lifetime in the human body of over a week.[27] Besides, they are supposedly not very susceptible to fragmentation or biodegradation. Prolonged clearance time risks patients experiencing an extended light-sensitive period after treatment when they suffer from skin and eye irritations. So far, gold nanostructures that can absorb NIR are single-particle-based designed. Their NIR absorption originates from particular shape-induced plasmon mode or from coupling between plasmon modes within the particle. Herein, we design a ″smart″ gold nanoparticle that can shift the absorption to far-red or NIR as it is aggregated in tumors. Coupled surface plasmons in closely located gold nanoparticles are exploited for photothermal therapy application. Coupled plasmons between gold nanoparticles have been mostly used for colorimetric sensor applications.[1,2]

A pH-sensitive surface molecule is designed, as it can switch its charge from negative to positive under an acidic environment. Spherical gold nanoparticles of 10 nm in diameter are used to exploit the large absorption cross section, yet they are reasonably small to avoid limitations from bulkiness. The size is also suited well for potential active cancer targeting, for example using antibodies, because of the optimal size for multivalent effect.[28] Gold nanoparticles are decorated with the pH-sensitive surface molecules. We refer to it as a ″smart″ gold nanoparticle since it can respond to reduced pH environments such as in the endosomal area of cancerous cells. It aggregates under acidic pH and shifts the absorption to far-red and NIR. Similarly to our case, absorption shift of gold nanoparticles upon aggregation or assembly has been reported using pH-dependent conformational changes of polypeptide surface molecules.[29,30] The conditional absorption shift to extended wavelengths can be well taken advantage of for maximal tissue penetrations in photothermal therapies. Cancer phototherapies can be advantageous in selectivity because photosensitizers become active only when being illuminated around the tumor mass. ″Smart″ gold nanoparticles can have additional selectivity because they become active only when aggregated in tumors and illuminated from outside, which can destroy cancer cells more selectively over normal cells. Strategic accumulations in tumor are expected for ″smart″ gold nanoparticles. On a cellular level, they can be rapidly accumulated inside of cancerous cells because exocytosis of the internalized nanoparticles can be effectively blocked as they form aggregates inside. On the tissue level, the gold nanoparticles can form aggregates in cores of tumor tissues that are usually acidic by hypoxia.[31] The aggregates can remain in the cores by enhanced retention.[32]

Result and Discussion

The pH-sensitive surface molecule was synthesized as shown in Scheme 1. It has a pH-sensitive citraconic amide moiety and a dithiol group for secure gold surface anchoring. Detailed synthetic procedures and full characterizations can be found in the Supporting Information. Citraconic anhydride is an R-methyl derivative of maleic anhydride, which is usually used for reversible blocking of amino groups in proteins.[33] When reacted with primary amines, citraconic anhydrides form amide bonds as shown in Scheme 1b. The amide bonds are stable under neutral or basic conditions, but they tend to hydrolyze abruptly at a pH lower than 7.0. Upon hydrolysis, **2** in Scheme 1 is converted back to **1** as it produces the citraconic acid. As a

(19) Oldenburg, S. J.; Averitt, R. D.; Westcott, S. L.; Halas, N. J. *Chem. Phys. Lett.* **1998**, *288*, 243–247.
(20) Sun, Y.; Xia, Y. *J. Am. Chem. Soc.* **2004**, *126*, 3892–3901.
(21) Huang, X.; El-Sayed, I. H.; Qian, W.; El-Sayed, M. A. *J. Am. Chem. Soc.* **2006**, *128*, 2115–2120.
(22) Hirsch, L. R.; Stafford, R. J.; Bankson, J. A.; Sershen, S. R.; Rivera, B.; Price, R. E.; Hazle, J. D.; Halas, N. J.; West, J. L. *Proc. Natl. Acad. Sci. U.S.A.* **2003**, *100*, 13549–13554.
(23) Loo, C.; Lowery, A.; Halas, N.; West, J.; Drezek, R. *Nano Lett.* **2005**, *5*, 709–711.
(24) Chen, J.; Wang, D.; Xi, J.; Au, L.; Siekkinen, A.; Warsen, A.; Li, Z.-Y.; Zhang, H.; Xia, Y.; Li, X. *Nano Lett.* **2007**, *7*, 1318–1322.
(25) Alkilany, A. M.; Nagaria, P. K.; Hexel, C. R.; Shaw, T. J.; Murphy, C. J.; Wyatt, M. D. *Small* **2009**, *5*, 701–708.
(26) Chithrani, B. D.; Ghazani, A. A.; Chan, W. C. W. *Nano Lett.* **2006**, *6*, 662–668.
(27) Choi, H. S.; Liu, W.; Misra, P.; Tanaka, E.; Zimmer, J. P.; Ipe, B. I.; Bawendi, M. G.; Frangioni, J. V. *Nat. Biotechnol.* **2007**, *25*, 1165–1170.
(28) Lytton-Jean, A. K. R.; Mirkin, C. A. *J. Am. Chem. Soc.* **2005**, *127*, 12754–12755.
(29) Shim, J.-Y.; Gupta, V. K. *J. Colloid Interface Sci.* **2007**, *316*, 977–983.
(30) Walker, D. A.; Gupta, V. K. *Nanotechnology* **2008**, *19*, 435603.
(31) Goode, J. A.; Chadwick, D. J. *The Tomour Microenvironment: Causes and Consequences of Hypoxia and Acidity*; John Wiley & Sons Ltd; New York, 2001.
(32) O'Neal, D. P.; Hirsch, L. R.; Halas, N. J.; Payne, J. D.; West, J. L. *Cancer Lett.* **2004**, *209*, 171–176.
(33) Brinegar, A. C.; Kinsella, J. E. *J. Agric. Food Chem.* **1980**, *28*, 818–824.

result, the surface molecule **3** can switch its charge from negative to positive as its terminal functional group changes from a carboxylate anion to protonated amine.

Gold nanoparticles 10 nm in diameter were made by following a conventional citrate method. An aqueous solution of hydrogen tetrachloroaurate was refluxed with sodium citrate to obtain citrate gold nanoparticles (see Supporting Information for experimental details).[34] The size was measured by TEM, and the hydrodynamic size was determined as being 12 nm by dynamic light scattering measurement (see Figures S3 and S4 in Supporting Information). Excess amounts of pH-sensitive surface molecules **3** were introduced to the citrate gold nanoparticles for surface exchange (see Supporting Information for experimental details). A slight red shift (~4 nm) is observed in the absorption spectrum after surface exchange, presumably due to the damping effect of the dithiol anchoring group on the gold surface (see Figure S5 in Supporting Information).[35] ″Smart″ gold nanoparticles show an enhanced colloidal stability over citrate gold nanoparticles. ″Smart″ and citrate gold nanoparticles were placed under high salt conditions of a 100 mM NaCl aqueous solution. While citrate gold nanoparticles quickly aggregate within a minute, ″smart″ gold nanoparticles survive without aggregations or flocculations (see Figure S6 in Supporting Information). The enhanced colloidal stability is ascribed to the secure surface anchoring of the dithiol group in the surface molecule. Since citraconic amide is susceptible to hydrolysis at a pH lower than 7.0, ″smart″ gold nanoparticles are expected to change their surface charges from negative to positive under acidic conditions. The hydrolysis lifetime of the citraconic amide bond was reported as being ~2 h at pH 5.5 and 35 °C.[33] ″Smart″ gold nanoparticles are supposed to have mixed surface charges during hydrolysis of the surface molecules. This results in rapid aggregations between nanoparticles. It is noted that the hydrolysis kinetics is adequate for our application. If it being too fast, aggregation would not be efficient because of the repulsions between fully surface charge converted nanoparticles. Proof of the concept for the ″smart″ nanoparticle was first demonstrated in buffer solutions. ″Smart″ gold nanoparticle solutions (3 nM) were prepared in 10 mM pH 5.5 acetate buffer (Figure 1A) and in 10 mM pH 7.4 phosphate buffer (Figure 1B), and their absorptions were monitored at 37 °C. Initially, both samples show their absorption peaks at 524 nm. The pH 5.5 sample shows a continuous red shift of the absorption with broadening over time. Broadening is ascribed to the appearance of coupled plasmon modes and inhomogeneity of the aggregates. The absorption peak shifts down to ~650 nm after 90 min, with its red side tail reaching over 800 nm. On the other hand, the pH 7.4 sample shows no noticeable absorption changes up to 120 min. This is clearly indicative of pH-induced aggregation of ″smart″ gold nanoparticles. It is further demonstrated that the aggregation of ″smart″ gold nanoparticles can be also active in complex media. When compared to Figure 1A, ″smart″ gold nanoparticles show similar aggregation patterns in 10% bovine serum albumin acetate buffer solutions of pH 5.5 (Figure 1C). This promises that the interactions between charged nanoparticles can prevail *in vivo* where various interferences by electrostatic attractions with biomolecules are expected. We also investigated the colloidal stability of ″smart″ gold nanoparticles in 100% bovine serum and in cell growth medium. To obtain the sizing and stability data of ″smart″ gold nanoparticles, the absorption change was monitored for up to 24 h. No noticeable changes in absorption were found, which is indicative of the colloidal stability. Hydrodynamic size measurements also confirmed the colloidal stability (see Figures S7 and S8 in Supporting Information). As a control, citrate gold nanoparticles were placed in pH 5.5 buffer by an identical method (Figure 1D). No noticeable absorption changes were observed over time except slight red tailing. The tailing is presumably due to slight aggregations of the nanoparticles by the colloidal instability. Figure 1E shows ″smart″ gold nanoparticle samples dispersed in pH 5.5 buffers for different elapsed times. As the absorption shifts to longer wavelengths over time, the color of the sample changes from red to violet and light blue. Hydrodynamic sizes were measured over time for the ″smart″ gold nanoparticle samples at pH 5.5 (Figure 1F). Initially the hydrodynamic size is 14 nm. After 10 min, it becomes 26 nm, which means the dimer is the majority. It reaches 41 nm at 30 min and 47 nm at 60 min. After 90 min, the hydrodynamic size becomes 443 nm, which suggests rapid merging between aggregates. Time evolutions of ″smart″ gold nanoparticle aggregates were further studied by dark field optical microscopy and TEM (Figure 1G). Under a dark field microscope, scatters change their color from green to orange and red, as larger aggregates are formed over time. The size and brightness of scatters become larger and stronger as well, as the aggregates scatter more light. TEM measurements confirm the growth of aggregates over time. The aggregation is thought to originate from electrostatic attractions between ″smart″ gold nanoparticles with mixed surface charges, when the hydrolysis of their surface molecules is in progress. A detailed illustration of the electrostatic attractions between ″smart″ gold nanoparticles can be found in the Supporting Information (see Figure S9 in Supporting Information). Once aggregated, ″smart″ gold nanoparticles do not easily turn back to individual nanoparticles. The aggregates are stable over hours even under acidic conditions, showing stabilities against hydrolysis. This enhanced stability of aggregates might result from the expected hydrophobic environment between aggregated gold nanoparticles that can expel water molecules. Aggregations by electrostatic attractions usually need two different kinds of particles with opposite charges. However, the dynamic nature of the ″smart″ gold nanoparticle surface enables the programmed aggregation by itself. We have also performed a control experiment to exclude the possibility that completely hydrolyzed ″smart″ gold nanoparticles may lose the colloidal stability and form aggregates. Completely hydrolyzed ″smart″ gold nanoparticles should have totally aminated surfaces. To mimic the case, primary amine-coated gold nanoparticles were made using *N*-(2-aminoethyl)-5-(1,2-dithiolan-3-yl)pentanamide (**1** in Scheme 1). Detailed synthesis of the surface molecule and the surface molecule exchange procedures can be found in the Supporting Information. It is noted that the primary amine-coated gold nanoparticle is exactly what the ″smart″ gold nanoparticle turns into after complete hydrolysis of the surface molecules. The primary amine-coated gold nanoparticles were dispersed under mild acidic buffer conditions such as pH 4 and 6 buffers. They showed no noticeable aggregations when monitored by the absorption for up to 120 min (see Figure S10 in Supporting Information). It is noted that ″smart″ gold nanoparticles show a progressive absorption shift under mild acidic conditions such as in pH 5.5 buffer solution (Figure 1A). However, the primary amine-coated gold nanoparticles are not colloidally stable at pH 9 because the primary amines are no longer protonated (thus positively charged) at the pH that reaches the pK_a of the primary

(34) Ji, X.; Song, X.; Li, J.; Bai, Y.; Yang, W.; Peng, X. *J. Am. Chem. Soc.* **2007**, *129*, 13939–13948.
(35) Moores, A.; Goettmann, F. *New J. Chem.* **2006**, *30*, 1121–1132.

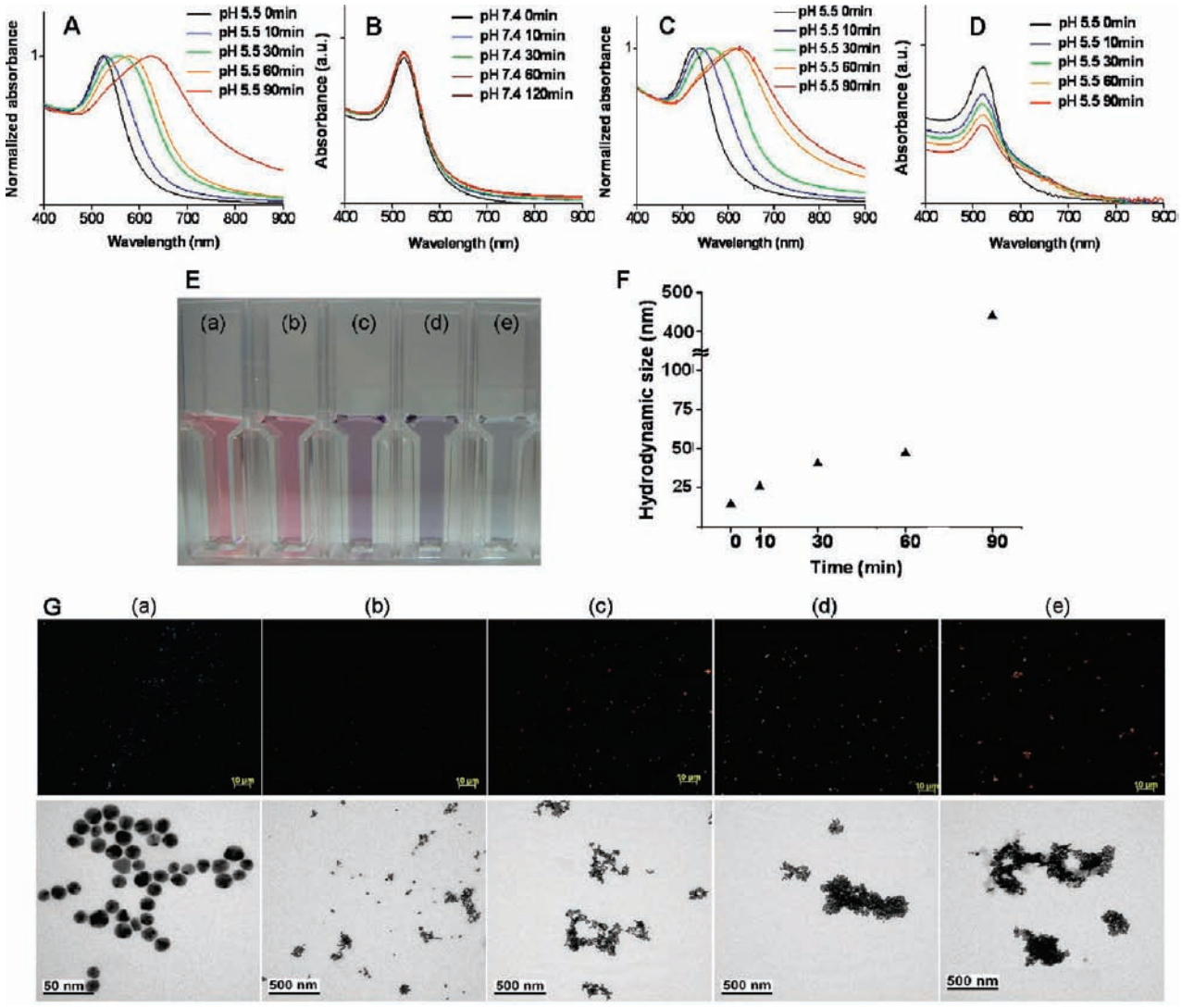

Figure 1. pH-induced aggregation of ″smart″ gold nanoparticles. Time evolutions of absorption for ″smart″ gold nanoparticles (A) in 10 mM pH 5.5 acetate buffer, (B) in 10 mM pH 7.4 phosphate buffer, (C) in 10% bovine serum albumin acetate buffer solution of pH 5.5; (D) Absorption spectra of citrate gold nanoparticles under 10 mM pH 5.5 acetate buffer condition; (E) Photograph of ″smart″ gold nanoparticle samples in pH 5.5 acetate buffer with different elapsed times of (a) 0, (b) 10, (c) 30, (d) 60, (e) 90 min; (F) hydrodynamic sizes of the samples (a) to (e), from left to right; (G) Dark field optical microscope images (top row) and TEM images (bottom row) of samples (a) to (e).

amine. To investigate the properties of cationic coated nanoparticles at pH 9 as well as at pH 4 and pH 6, we have also synthesized quaternary amine-coated gold nanoparticles. Detailed synthesis of the surface molecule and the surface molecule exchange procedures can be found in the Supporting Information. The quaternary amine-coated gold nanoparticles were dispersed in pH 4, 6, and 9 buffer solutions. They did not show any noticeable changes in absorption over time (see Figure S11 in Supporting Information). This demonstrates the colloidal stability of cationic coated gold nanoparticles.

Since pH-induced aggregation was confirmed for ″smart″ gold nanoparticles, they were further applied to cellular applications. Most cells, especially cancerous ones including B16 F10 mouse melanoma cells, are known to internalize nanoparticles. They can engulf nanoparticles through receptor-mediated endocytosis or membrane rupturing on nonspecific bindings. B16 F10 cells were incubated with ″smart″ gold nanoparticles in MEM/EBSS which were supplemented with 10% FBS and 1% PS at 37 °C under 5% CO_2. Citrate gold nanoparticles and 11-mercaptoundecanoic acid (MUA)-capped gold nanoparticles were used for control groups (see Supporting Information for experimental details). When foreign molecules are internalized into cells via an endocytic pathway, they are exposed to acidic environments as endocytic vesicles changed from early and late endosomes to lysosomes.[36] ″Smart″ gold nanoparticles can respond to the pH change and form aggregates. As shown in Figure 1G, formation and growth of gold nanoparticle aggregates can be monitored using dark field microscopy. Figure 2 shows dark field images of B16 F10 cells incubated with ″smart″ gold nanoparticles (first column), citrate gold nanoparticles (second column), and MUA-capped gold nanoparticles (third column). Efficient accumulation of ″smart″ gold nanoparticle aggregates is observed in B16 F10 cells, appearing as strong orange scatters. It is noted that the dark field microscope images of aggregates in cells are very similar to those in Figure 1G. Morphologies of cells are clearly visualized by the bright scattering of nanoparticle aggregates inside. The aggregate accumulation

(36) Bae, Y.; Fukushima, S.; Harada, A.; Kataoka, K. *Angew. Chem., Int. Ed.* **2003**, *42*, 4640–4643.

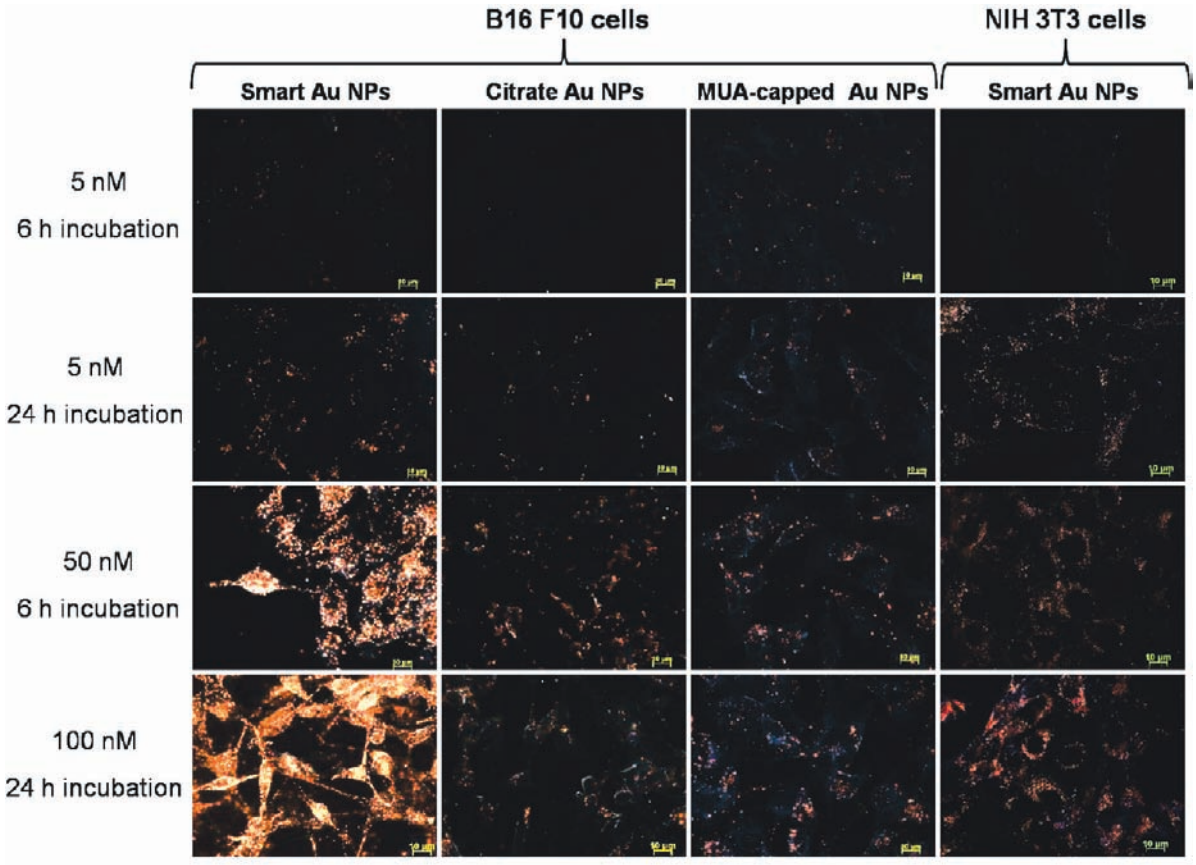

Figure 2. Dark field microscope images of B16 F10 cells and NIH 3T3 cells. B16 F10 cells were incubated with ″smart″ gold nanoparticles (first column), citrate gold nanoparticles (second column), and MUA-capped gold nanoparticles (third column). NIH 3T3 cells were incubated with ″smart″ gold nanoparticles (last column). The nanoparticle concentration/incubation time (nM/h) is 5/6, 5/24, 50/6, and 100/24 from top to bottom row.

increases at a higher nanoparticle concentration or longer incubation time. In contrast, small scatterings are observed for control gold nanoparticle samples. Most citrate gold nanoparticles are thought to stay individually even after being internalized into the cells. Because of the small scattering cross section of individual gold nanoparticles, they are not well visualized. Small numbers of scattering aggregates in citrate gold nanoparticle samples are presumably due to aggregations by the colloidal instability. This also agrees with our result in Figure 1D. MUA-capped gold nanoparticles were used for another control group since they have a covalently bound carboxylic terminal group as ″smart″ gold nanoparticles do and are colloidally more stable than citrate gold nanoparticles. We find no significant difference from citrate gold nanoparticles. To further investigate the enhanced cellular accumulation of ″smart″ gold nanoparticles, confocal microscope images were acquired using B16 F10 cells that had been incubated respectively with 100 nM ″smart″ or MUA-capped gold nanoparticles for 24 h (see Figure S12 in Supporting Information). ″Smart″ gold nanoparticle treated cells show bright scatterings at the *z*-scanning. This is due to the massively accumulated aggregates of the ″smart″ gold nanoparticles. In contrast, no noticeable scatterings can be found in the case of MUA-capped gold nanoparticle treated cells, which is also in accordance with the result in Figure 2. To exclude the possibility that MUA-capped gold nanoparticles lose colloidal stability in cell growth medium and fail to internalize into the cells, the colloidal stability of MUA-capped gold nanoparticles in cell growth medium was also studied in vitro by monitoring the absorption changes. Experimental conditions identical to those for the samples in Figure 2 were used except there was no cell present. No noticeable changes were found in the absorption up to 24 h, indicating the colloidal stability of MUA-capped gold nanoparticles in the cell growth medium (see Figure S13 in Supporting Information). This proves that the control groups do not show bright scatterings under a dark field microscope or confocal microscope because of the lack of ability to form aggregates inside of cells and not because of the colloidal instability. As a normal cell control against the B16 F10 cells, NIH 3T3 mouse embryonic fibroblast cells were incubated with ″smart″ gold nanoparticles (Last column in Figure 2). Although there are significant accumulations of ″smart″ gold nanoparticles in NIH 3T3 cells, the accumulations were not as efficient as B16 F10 cells. The intracellular environment of normal cells can be also acidic and can cause aggregations and accumulations of ″smart″ gold nanoparticles. However, ″smart″ gold nanoparticles show cancer specificity over normal cells presumably because of the unique phagocytic activities of cancer cells. As expected, ″smart″ gold nanoparticles internalize into cells, change their surface charges, form aggregates, and accumulate inside of the cells. As they form aggregates, exocytosis should be effectively blocked by the size effect.[37] It is noted that identical gold nanoparticles are used for all cases except the surface molecules and that the surfaces are negatively charged for all cases. This suggests the internalization efficiency should be similar for all cases. It is demonstrated that the accumulation

(37) Chithrani, B. D.; Chan, W. C. W. *Nano Lett.* **2007**, *7*, 1542–1550.

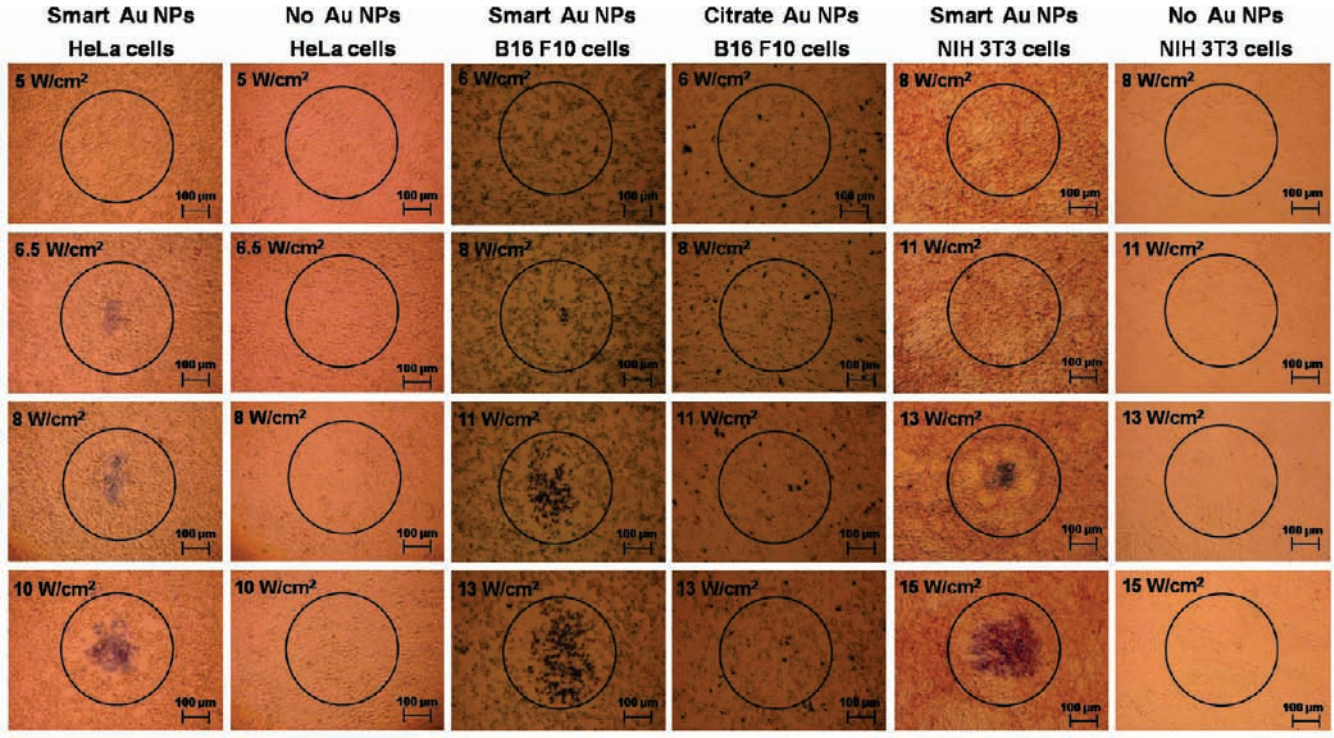

Figure 3. Photothermal destruction of cells. HeLa cells were incubated with ″smart″ gold nanoparticles (first column) and with no nanoparticles (second column). B16 F10 cells were incubated with ″smart″ gold nanoparticles (third column) and with citrate gold nanoparticles (fourth column). NIH 3T3 cells were incubated with ″smart″ gold nanoparticles (fifth column) and with no nanoparticles (last column). Laser fluence rates are 5, 6.5, 8, and 10 W/cm^2 for HeLa cells; 6, 8, 11, and 13 W/cm^2 for B16 F10 cells; and 8, 11, 13, and 15 W/cm^2 for NIH 3T3 cells, respectively, from top to bottom row. Circles denote the position of laser spot.

of ″smart″ gold nanoparticle aggregates inside of the cells results from the pH-responding surface molecules.

We have successfully showed that ″smart″ gold nanoparticles can efficiently accumulate and form aggregates inside of cells. The aggregates absorb far-red and NIR, which can be taken advantage of for photothermal therapies guaranteeing maximal tissue penetrations. This can help photothermal therapies to reach more internally existing organs. It was further studied if the accumulated ″smart″ gold nanoparticle aggregates can efficiently destroy cancerous cells in response to external illumination. HeLa (Human cervical cancer cell) and B16 F10 cells were used. Gold nanoparticles were incubated with HeLa cells in Dulbecco's Modified Eagle Medium (DMEM) and with B16 F10 cells in MEM/EBSS. The media were supplemented with 10% FBS and 1% PS at 37 °C under 5% CO_2 (see Supporting Information for experimental details). ″Smart″ gold nanoparticles (60 nM) were incubated with HeLa cells for 24 h (First column in Figure 3). A CW diode laser of 660 nm was used for illumination. It is noted that ″smart″ gold nanoparticles cannot absorb this wavelength until they aggregate. Circles in Figure 3 represent the position of laser spots. The spot has an ∼500 μm radius, as is measured using photosensitive paper. A control sample was incubated without any nanoparticles (second column in Figure 3). Both samples were illuminated for 10 min using different laser power densities of 5, 6.5, 8, and 10 W/cm^2. Trypan blue was used to reveal the mortality of cells with blue staining. In the case of ″smart″ gold nanoparticle treated cells, mortal cells appear at a laser power of 6.5 W/cm^2 or higher. The circular areas of damaged cells increase linearly with the irradiation power density. On the other hand, no noticeable mortal cells are found for the control group and for the cells outside of the laser spot. It is noted that threshold behavior for photothermal therapy is observed for ″smart″ gold nanoparticles. The threshold should lie between 5 and 6.5 W/cm^2. A similar experiment was performed using B16 F10 cells. ″Smart″ gold nanoparticles (100 nM) were used for co-incubation (third column in Figure 3), and citrate gold nanoparticles (100 nM) were used as a control group (fourth column in Figure 3). ″Smart″ gold nanoparticle treated cells show mortality at laser illuminations higher than 8 W/cm^2. In contrast, no noticeable mortal cells were found for the citrate gold nanoparticle treated cells and for the cells outside of the laser spot, regardless of the laser fluence power. The ″smart″ gold nanoparticles show selective and efficient destruction of cancerous cells with an intensity threshold of 8 W/cm^2 to induce the thermal destruction. In the intensity range 8−13 W/cm^2, the circular areas of damaged cells increase linearly with the irradiation power density. As expected, citrate gold nanoparticles do not readily form aggregates inside of cells and fail to efficiently absorb the laser light. Randomly positioned aggregates of citrate gold nanoparticles were observed as black spots. NIH 3T3 cells were used as a normal cell line against B16 F10 cells (fifth column in Figure 3). A control sample was incubated without any nanoparticles (last column in Figure 3). Gold nanoparticles were incubated with NIH 3T3 cells in DMEM supplemented with 10% FBS and 1% PS at 37 °C under 5% CO_2. ″Smart″ gold nanoparticle treated cells begin to show mortality at a threshold laser power density of 13 W/cm^2. This is higher than the 8 W/cm^2 threshold for B16 F10 cells. The higher threshold for NIH 3T3 cells is thought to result from the less efficient accumulation of ″smart″ gold nanoparticles as shown in Figure 2. Cancer cells are also known to be more susceptible to heat shock. This may also have contributed to the higher threshold of normal cells (NIH 3T3) over cancer cells (B16 F10). The circular area of damaged cells increases as the

irradiation power density increases to 15 W/cm^2. No detectable cell mortality was found at the area outside of the laser spot regardless of the illumination power, which is indicative of the minimal dark cytotoxicity. No noticeable mortal cells were found for the control group that was incubated with no gold nanoparticle. It is stressed that our modality can have selectivity at the cellular level, since cells that are not treated with gold nanoparticles or that are treated with citrate gold nanoparticles do not show mortality even at higher laser fluence than the threshold for ″smart″ gold nanoparticle treated cells. We have also performed a concentration and time dependent cytotoxicity assay for ″smart″ gold nanoparticles (see Supporting Information for experimental details). B16 F10 cells were incubated with ″smart″ gold nanoparticles, and the survival rate was evaluated by the mitochondrial activity. No noticeable cytotoxicities by ″smart″ gold nanoparticles were found up to 100 nM for 24 h (see Figure S14 in Supporting Information).

It is noted that our threshold fluence dose is less than or comparable to the cases of nanorods[21] or nanoshells.[22,23] The comparison of thresholds is made on the assumption that cells are saturated with the nanoparticles by the treatment conditions such as nanoparticle concentration and incubation time. It is stressed that the ″smart″ gold nanoparticle is smallest in size among the above-mentioned nanostructures. The ″smart″ gold nanoparticle is at least more than an order of magnitude smaller in volume than other nanostructures. The scattering cross section is typically proportional to the particle volume. The photothermal efficacy of our ″smart″ gold nanoparticle is relatively high despite the small size because of its ability to form aggregates that can efficiently utilize the illumination. It is also noted that the ″smart″ gold nanoparticles do not yet have active cancer targeting moieties such as antibodies. Still, they show a photothermal threshold that is smaller or comparable to those of other actively targeting nanostructures.[21−23] Conjugation of active cancer targeting groups to ″smart″ gold nanoparticles can be achieved by a mixed surface molecule system or by conjugation at the end of the citraconic amide group. This is currently in progress along with the possibility of conjugating conventional anticancer drug molecules onto the citraconic amide terminals for conditional drug release inside of cancerous cells. This will be reported in forthcoming publications. We expect that the photothermal threshold will be further lowered by the active targeting group conjugation to our ″smart″ gold nanoparticles.

″Smart″ gold nanoparticles show efficient photothermal efficacy with a very low fluence illumination threshold. This is somewhat surprising considering the small scattering cross section by the small size and its absence of active targeting group. This can be ascribed to the efficient internalization of ″smart″ gold nanoparticles by their small size and the aggregation-induced accumulations. Since ″smart″ gold nanoparticles are very small in size, their biodistribution and clearance pathway can be potentially well controlled. Additionally, smaller particles can simply mean smaller amounts of exogenous materials to patients when the same concentration is administered.

Conclusions

We have successfully designed and synthesized a ″smart″ gold nanoparticle that can respond to pH change and form aggregates. When exposed to an acidic environment or internalized inside of cells, ″smart″ gold nanoparticles begin to aggregate. This results in rapid formation of mixed charged particle surfaces, which results in the formation and growth of ″smart″ gold nanoparticle aggregates. Enhanced accumulations of ″smart″ gold nanoparticles by blocked exocytosis are clearly visualized by dark field microscopy. The pH-induced aggregates shift their absorption to far-red and NIR. This absorption shift is exploited for photothermal cancer therapy. Using B16 F10 mouse melanoma, NIH 3T3 mouse embryonic fibroblast cells, and HeLa cells, the photothermal efficacy of ″smart″ gold nanoparticles is demonstrated. No noticeable dark toxicity is found, and a sharp contrast is observed for the efficacy over the control groups that used citrate gold nanoparticles or that treated with no gold nanoparticle. ″Smart″ gold nanoparticles show a relatively low power threshold for photothermal therapy, promising a new efficient modality for *in vivo* animal models and future clinical trials.

Acknowledgment. This work was supported by the Korea Research Foundation Grant funded by the Korean Government-(MOEHRD) (KRF-2008-005-J00501, KRF-2008-331-C00140), Ministry of Health & Welfare (A060660), and Korea Science and Engineering Foundation (KOSEF) grant funded by the Korea government(MOST) (M10755020003-07N5502-00310, M10703001036-08M0300-03610, and R0A-2008-000-20114-0(2008)).

Supporting Information Available: Details of experimental procedures and TEM images, size distributions, absorption spectra of ″smart″ and citrate gold nanoparticles, illustration of aggregation process of ″smart″ gold nanoparticles. Colloidal stability experiments of gold nanoparticles with various surfaces. Confocal microscopic images of ″smart″ gold nanoparticle incubated cells and the control MUA-capped gold nanoparticle incubated cells. Concentration and time dependent viability assay results on ″smart″ gold nanoparticle treated cells. This material is available free of charge via the Internet at http://pubs.acs.org.

JA902062J